01 Mar 1996

A Magnetic Neutron Diffraction, and Mössbauer Spectral Study of the $Ce_2Fe_{17-x}Al_x$ Solid Solutions

Sanjay R. Mishra

Gary J. Long
Missouri University of Science and Technology, glong@mst.edu

Oran Allan Pringle
Missouri University of Science and Technology, pringle@mst.edu

D. P. Middleton

et. al. For a complete list of authors, see https://scholarsmine.mst.edu/chem_facwork/776

Recommended Citation

S. R. Mishra et al., "A Magnetic Neutron Diffraction, and Mössbauer Spectral Study of the $Ce_2Fe_{17-x}Al_x$ Solid Solutions," *Journal of Applied Physics*, vol. 79, no. 6, pp. 3145-3155, American Institute of Physics (AIP), Mar 1996.
The definitive version is available at https://doi.org/10.1063/1.361257

A magnetic, neutron diffraction, and Mössbauer spectral study of the $Ce_2Fe_{17-x}Al_x$ solid solutions

S. R. Mishra, Gary J. Long, and O. A. Pringle
Departments of Physics and Chemistry, University of Missouri-Rolla, Rolla, Missouri 65409-0010

D. P. Middleton
Philips Research Laboratories, NL-5656 AA Eindhoven, The Netherlands

Z. Hu and W. B. Yelon
University of Missouri Research Reactor and the Departments of Physics and Chemistry, University of Missouri-Columbia, Columbia, Missouri 65211

F. Grandjean
Institute of Physics, B5, University of Liège, B-4000 Sart-Tilman, Belgium

K. H. J. Buschow
Van der Waals-Zeeman Laboratory, University of Amsterdam, NL-1018 XE Amsterdam, The Netherlands

(Received 15 August 1995; accepted for publication 6 November 1995)

The magnetic properties of a series of $Ce_2Fe_{17-x}Al_x$ solid solutions with x equal to 0.00, 0.88, 2.06, 2.81, 3.98, 5.15, 6.08, 7.21, 8.20, 9.08, 9.84, and 10.62 have been studied by magnetic measurements, neutron diffraction, and Mössbauer spectroscopy. The compounds crystallize in the rhombohedral Th_2Zn_{17}-type structure. Magnetization studies indicate that the Curie temperature increases uniformly from 238 K for Ce_2Fe_{17} to 384 K for $Ce_2Fe_{14}Al_3$ and then decreases at higher aluminum content. Powder neutron diffraction results, obtained at 295 K, indicate that aluminum avoids the $9d$ site for all x values and preferentially occupies the $18h$ site at low aluminum content. Aluminum shows a marked preference for the $6c$ site for $x>6$. The room-temperature iron magnetic moments increase from $x=0$ to 2 and then decrease for $x>2$. The Mössbauer spectra have been fit with a binomial distribution of the near-neighbor environments in terms of a maximum hyperfine field, $H_{\max}$, for an iron with zero aluminum near neighbors, and a decremental field, ΔH, per aluminum near neighbor. The compositional dependence of the decremental field indicates the influence of aluminum on the long-range magnetic ordering in the compound. The compositional dependence of the weighted average maximum hyperfine fields and the weighted average isomer shifts in $Ce_2Fe_{17-x}Al_x$ may be understood in terms of a mixing of the $3d$ conduction band electrons with the $3p$ valence band electrons of aluminum, a mixing which is more extensive than that associated with silicon in the $Ce_2Fe_{17-x}Si_x$ solid solutions. We conclude that this mixing has a larger influence on the magnetic properties of these solid solutions than does the presence of a short iron–iron bond or the expansion or contraction of the lattice parameters and unit cell volume. © *1996 American Institute of Physics.* [S0021-8979(96)00804-8]

I. INTRODUCTION

Iron-based compounds with the rhombohedral Th_2Zn_{17} structure have high saturation magnetizations.[1] Unfortunately, the relatively low Curie temperatures and low magnetocrystalline anisotropies of the R_2Fe_{17} compounds make them less attractive for applications as permanent magnet materials. The low Curie temperatures are usually attributed to negative exchange interactions between iron atoms situated at very short distances from each other.[2] The interstitial insertion of nitrogen[3] and carbon[4,5] into the R_2Fe_{17} structure produces considerable improvement in the hard magnetic properties of the binary compounds. In the interstitial compounds, the iron–iron distances are increased as compared to those found in the binary compounds, an increase which substantially increases their Curie temperatures. Unfortunately, although these interstitial compounds appear to be promising permanent magnetic materials, they are thermodynamically unstable and decompose into rare-earth nitrides or carbides and α-iron at high temperatures. Thus, the processing of these compounds, for instance by sintering, is difficult. An alternative route to increased bond distances, and hence Curie temperatures, is to force the lattice to expand by replacing iron by an element with a larger metallic radius, such as gallium or aluminum.[6]

Cerium, the least expensive of all the rare-earth elements, when present in the trivalent state, can give rise to rare-earth anisotropies much larger than those of the other rare-earth elements[7] in intermetallic compounds. However, cerium has a tendency to be close to tetravalent[8] when combined with $3d$ metals, a tendency which limits the application of most cerium-based intermetallic compounds as permanent magnetic materials. We have previously reported[9] that an improvement in the Ce_2Fe_{17} magnetic properties can be brought about by the substitution of a nonmagnetic atom, such as silicon, a substitution which expands the c axis, contracts the a axis, and contracts the $6c-6c$ iron–iron distance. The increase in the Curie temperature of Ce_2Fe_{17} upon substitution of silicon for iron provides direct evidence that the expansion of the unit cell volume and the $6c-6c$ iron–

TABLE I. The lattice and positional parameters, site occupancies, and magnetic moments in $Ce_2Fe_{17-x}Al_x$ as measured by neutron diffraction at 295 K.

x, refined	0.00	0.88	2.06	2.81	3.98	5.15	6.08	7.21	8.20	9.08	9.84	10.62
a, Å	8.492 1(2)	8.539 4(3)	8.572 5(4)	8.610 4(2)	8.644 7(4)	8.676 5(2)	8.715 1(4)	8.759 5(3)	8.801 9(3)	8.839 2(3)	8.884 7(5)	8.928 1(8)
c, Å	12.406 0(3)	12.466 4(4)	12.514 5(6)	12.575 2(3)	12.626 5(6)	12.668 5(4)	12.709 4(6)	12.747 6(5)	12.781 0(5)	12.839 3(5)	12.919 2(8)	12.981 2(13)
c/a	1.460 9(1)	1.459 9(1)	1.459 8(1)	1.460 5(1)	1.460 6(1)	1.460 1(1)	1.458 3(1)	1.455 3(1)	1.452 1(1)	1.452 5(1)	1.454 1(2)	1.454 0(3)
V, Å^3	774.81(6)	787.27(8)	796.45(11)	807.41(6)	817.17(11)	825.93(6)	835.99(11)	847.07(9)	857.53(9)	868.76(9)	883.19(15)	896.09(25)
Ce, 6c, z	0.344 1(5)	0.342 5(8)	0.339 7(9)	0.342 0(6)	0.344 0(8)	0.344 6(5)	0.345 3(6)	0.345 4(5)	0.347 9(4)	0.347 2(4)	0.346 4(6)	0.344 1(9)
Fe/Al, 6c, z	0.097 0(2)	0.096 3(3)	0.096 9(4)	0.096 3(2)	0.096 4(4)	0.097 0(3)	0.097 6(4)	0.099 7(3)	0.103 1(4)	0.103 6(5)	0.106 1(7)	0.103 8(11)
Fe/Al, 18f, x	0.290 5(1)	0.290 8(2)	0.291 3(3)	0.289 7(2)	0.289 3(3)	0.288 6(2)	0.287 7(3)	0.288 2(2)	0.288 5(2)	0.289 8(3)	0.289 6(4)	0.291 6(6)
Fe/Al, 18h, x	0.167 8(1)	0.168 3(2)	0.168 7(2)	0.169 2(2)	0.169 6(2)	0.169 9(2)	0.169 7(2)	0.169 1(2)	0.167 7(2)	0.168 0(2)	0.168 1(3)	0.169 1(4)
Fe/Al, 18h, z	0.488 3(1)	0.487 5(2)	0.487 6(2)	0.488 7(2)	0.489 0(3)	0.489 4(2)	0.488 9(2)	0.489 9(2)	0.490 7(2)	0.490 5(4)	0.489 4(2)	0.490 8(4)
% Al, 6c	0.0	4.2	8.4	11.4	22.2	28.7	37.7	59.9	83.8	91.6	96.4	100
% Al, 9d	0.0	0.0	0.0	0.0	0.0	0.0	0.0	0.0	0.0	0.0	0.0	0.0
% Al, 18f	0.0	2.8	8.6	11.8	18.8	31.8	40.0	53.8	66.2	74.6	79.0	84.0
% Al, 18h	0.0	10.4	23.0	31.2	40.2	44.0	48.6	46.4	42.0	46.0	52.8	59.8
R-factor	5.05	5.93	6.49	5.66	6.33	5.59	8.81	6.01	6.74	6.26	8.74	11.4
R_w-factor	7.11	7.04	7.73	7.52	7.41	7.45	11.10	7.92	8.50	8.24	11.0	15.7
R_m-factor	···	4.37	6.84	7.33	7.42	5.73	12.50	···	···	···	···	···
χ^2	2.91	2.23	3.70	3.98	2.34	2.78	3.66	2.87	2.68	3.53	3.61	7.37
μ_{Fe}, 6c, μ_B	0.0	1.2(2)	1.8(2)	1.6(2)	1.1(2)	0.9(4)[a]	0.3[b]	0.0	0.0	0.0	0.0	0.0
μ_{Fe}, 9d, μ_B	0.0	1.4(3)	1.8(2)	1.5(4)	1.5(3)	0.9(4)[a]	0.3[b]	0.0	0.0	0.0	0.0	0.0
μ_{Fe}, 18f, μ_B	0.0	1.1(3)	1.5(2)	1.3(2)	0.7(3)	0.9(4)[a]	0.3[b]	0.0	0.0	0.0	0.0	0.0
μ_{Fe}, 18h, μ_B	0.0	1.0(3)	1.0(2)	1.2(3)	0.8(3)	0.9(4)[a]	0.3[b]	0.0	0.0	0.0	0.0	0.0
μ_{Fe}, wt. avg., μ_B	0.0	1.1(3)	1.4(2)	1.4(3)	1.0(3)	0.9(4)	0.3	0.0	0.0	0.0	0.0	0.0
μ, formula, μ_B	0.0	18.3	21.5	19.2	12.5	10.7	3.3	0.0	0.0	0.0	0.0	0.0

[a]In this compound the individual iron site magnetic moments could not be refined independently.
[b]In this compound the free refinement of the iron site magnetic moments was not stable and the value shown was obtained by an iterative refinement.

iron distance are not the only factors involved in improving the magnetic properties of the rare-earth permanent magnets. As a continuing part of the investigation of the effect of nonmagnetic substitutional atoms on the microscopic properties of R_2Fe_{17} compounds we present herein the results of magnetic measurements, and neutron diffraction and Mössbauer spectral studies of the $Ce_2Fe_{17-x}Al_x$ solid solutions.

II. EXPERIMENTAL METHODS

The samples were prepared from 99.9% pure elements by arc melting in an argon atmosphere. After arc melting, the samples were wrapped in tantalum foil and were vacuum annealed in quartz tubes at 1170 K for two weeks. Their purities and structures were investigated by powder x-ray diffraction with CuK_α radiation on a Philips PW 1800/10 x-ray diffractometer equipped with a single-crystal monochromator. The $Ce_2Fe_{17-x}Al_x$ solid solutions were found to contain at most a few percent of α-iron as an impurity phase. The magnetic measurements were performed on field-cooled free particle samples in a superconducting quantum interference device (SQUID) magnetometer between 5 and 350 K and on a Faraday magnetometer between 350 and 1000 K. The Curie temperatures were determined in a magnetic field of 0.1 T by plotting the magnetization versus temperature and extrapolating the steepest part of the curve to zero magnetization. The values are believed to be accurate to ± 3 K. Values of the saturation magnetization at 5 K were obtained from the magnetic isotherms by extrapolating the $M(1/B)$ curves to $1/B=0$.

The powder neutron diffraction patterns were obtained by using a linear position sensitive detector and neutrons with a wavelength of 1.4783 Å. The data for each sample were collected at 295 K between 2θ angles of 5° and 105° on approximately 2 g of finely powdered sample placed in a thin wall vanadium container. Refinements of the neutron diffraction data were carried out with the FULLPROF code[10] which permits multiple phase refinement as well as magnetic structure refinement of coexisting phases, and refinement constraints which were the same as those used in our earlier work.[9,11]

The Mössbauer spectra were obtained on a constant-acceleration spectrometer which utilized a room-temperature rhodium matrix cobalt-57 source and was calibrated at room temperature with α-iron foil. The Mössbauer absorbers, which were $\sim$30 mg/cm^2, were prepared from powdered samples which had been sieved to a 0.045 mm or smaller particle diameter. The resulting spectra have been fit as discussed below and elsewhere[11] and the estimated errors are ± 2 kOe for the maximum hyperfine fields, H_{max}, and the decremental fields, ΔH, and ± 0.01 mm/s for the isomer shifts, δ. The hyperfine parameters for the α-iron phase were constrained to their known values.

III. RESULTS

The results of the refinement of the powder neutron diffraction patterns for $Ce_2Fe_{17-x}Al_x$ with refined x values of 0.0, 0.88, 2.06, 2.81, 3.98, 5.15, 6.08, 7.21, 8.20, 9.08, 9.84, and 10.62 are given in Table I. The neutron-diffraction derived unit cell parameters for the $Ce_2Fe_{17-x}Al_x$ solid solutions agree very well with those measured for the same samples by x-ray diffraction.[7] As shown in Fig. 1, the lengths of the a and c axes increase with x, with slopes of 0.039 and 0.049 Å per aluminum, respectively, values which are noticeably larger than the increases observed[9,12,13] in

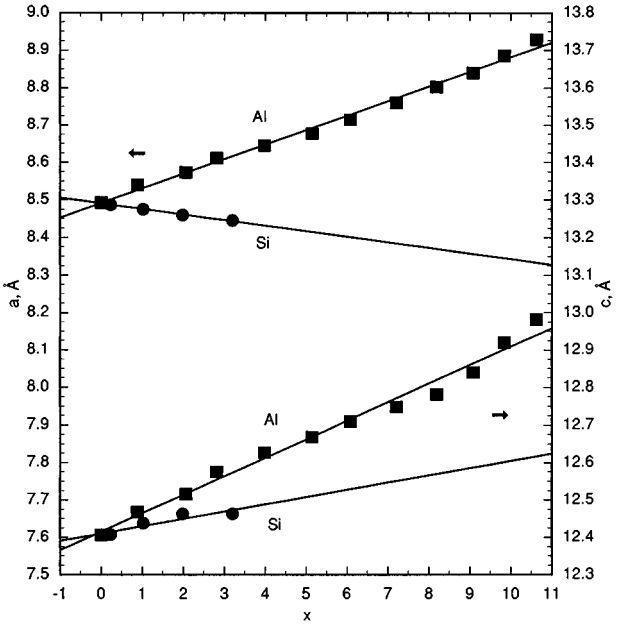

FIG. 1. The 295 K lattice parameters for the $Ce_2Fe_{17-x}Al_x$, ■, and $Ce_2Fe_{17-x}Si_x$, ●, solid solutions as a function of x.

$Nd_2Fe_{17-x}Al_x$, $Tb_2Fe_{17-x}Al_x$, and $Ce_2Fe_{17-x}Si_x$, the latter of which is shown for comparison in Fig. 1. The tendency of cerium to remain close to the tetravalent state[8] when forming a compound with the transition metals leads to smaller unit cell volumes for the $Ce_2Fe_{17-x}Al_x$ solid solutions than for $Nd_2Fe_{17-x}Al_x$ and $Tb_2Fe_{17-x}Al_x$ but larger volumes than for $Ce_2Fe_{17-x}Si_x$ (see Fig. 2). The unit cell volume shows a linear increase of 10.7 Å^3 per aluminum, an increase which is greater than the increase of 8.3 and 9.0 Å^3 per aluminum observed[12,13] in $Nd_2Fe_{17-x}Al_x$ and $Tb_2Fe_{17-x}Al_x$ and the

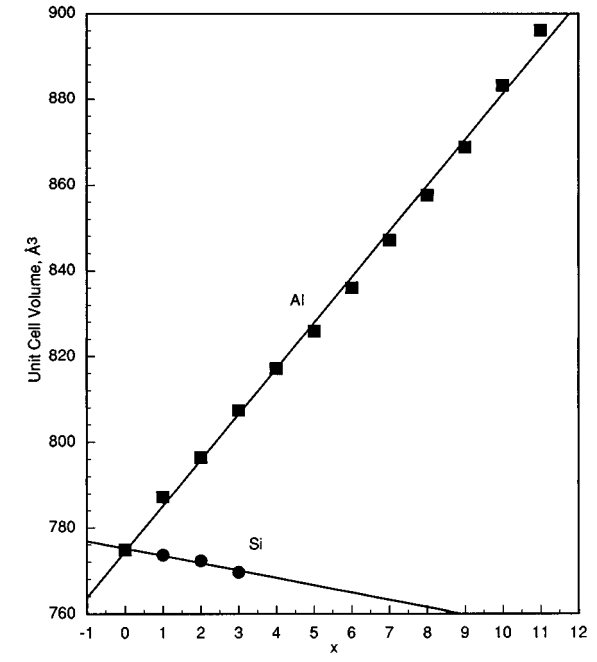

FIG. 2. The 295 K unit cell volume for the $Ce_2Fe_{17-x}Al_x$, ■, and $Ce_2Fe_{17-x}Si_x$ ●, solid solutions as a function of x.

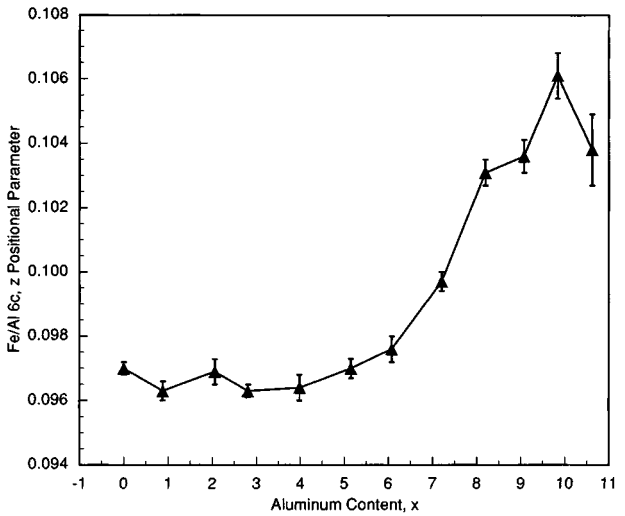

FIG. 3. The Fe/Al 6c, z positional parameter for the $Ce_2Fe_{17-x}Al_x$ solid solutions as a function of aluminum content.

value of −1.7 Å^3 per silicon observed[9] in $Ce_2Fe_{17-x}Si_x$. All of these values, except for the latter, are larger than the 7.2 Å^3 per nitrogen increase found[14] for the unit cell volume of Nd_2Fe_{17} upon nitrogenation to form $Nd_2Fe_{17}N_{2.4}$.

Even though the lattice parameters and unit cell volume of the $Ce_2Fe_{17-x}Al_x$ solid solutions increase linearly with increasing aluminum content, the positional parameters (see Table I) do not remain constant, or change linearly, with the exception of the Fe/Al 18h, z parameter, which increases linearly with aluminum content with a slope of 2.7×10^{-4} per aluminum. Indeed, as shown in Fig. 3, the Fe/Al 6c, z position remains relatively constant below $x=6$ and then increases substantially, whereas the Fe/Al 18f, x, and Fe/Al 18h, x positions show a broad minimum and maximum, respectively, centered at $x\approx6$. Very similar trends with aluminum content are also observed[12] in $Nd_2Fe_{17-x}Al_x$, but the trends[9] in $Ce_2Fe_{17-x}Si_x$ are different. These variations are well in excess of the error associated with these positions, even though these errors tend to increase with aluminum content. It should be noted that aluminum has a scattering length of 0.3449×10^{-12} cm which is substantially below the 0.954×10^{-12} cm length for iron. As a result of this difference the total unit cell scattering length decreases from 51.6×10^{-12} cm for Ce_2Fe_{17} to 32.2×10^{-12} cm for $Ce_2Fe_{6.38}Al_{10.62}$ and, as a consequence, the errors increase. The variation in the positional parameters is no doubt a result of the preferential occupancy pattern of aluminum in Ce_2Fe_{17} (see Fig. 4), a pattern which changes between $x=6$ and 7. Below $x=6$ aluminum prefers the 18h site and has little effect on the Fe/Al 6c, z position and hence the Fe/Al–Fe/Al 6c–6c bond distance increases only slightly because of the c-axis expansion (see Fig. 5). However, for $x>6$, aluminum prefers the Fe 6c and 18f sites and the presence of aluminum on these sites clearly increases the Fe/Al 6c, z position and thus the Fe/Al–Fe/Al 6c–6c bond distance. This trend is also observed, although at larger distances, for the Fe/Al–Fe/Al 6c–18f bond distance. As may be seen in Fig. 5, all

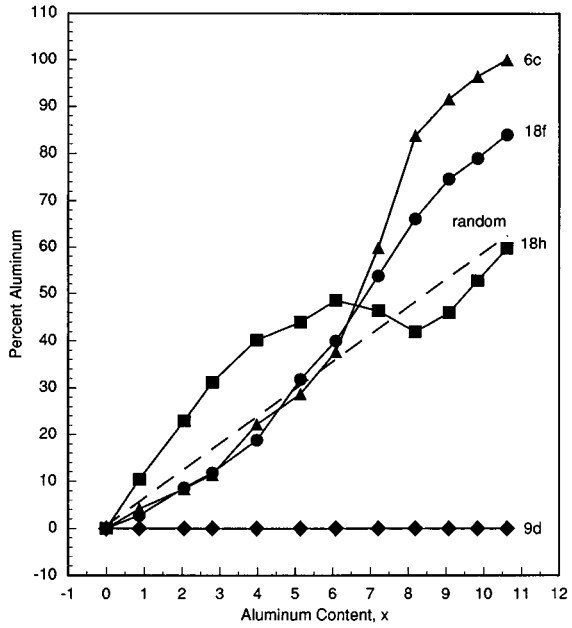

FIG. 4. The percentage of aluminum found on the four crystallographic iron sites in the $Ce_2Fe_{17-x}Al_x$ solid solutions as a function of aluminum content.

the other Fe/Al–Fe/Al bond distances increase approximately linearly with x.

The crystallographic site preference exhibited by aluminum in $Ce_2Fe_{17-x}Al_x$ (see Fig. 4 and Table I) is similar to

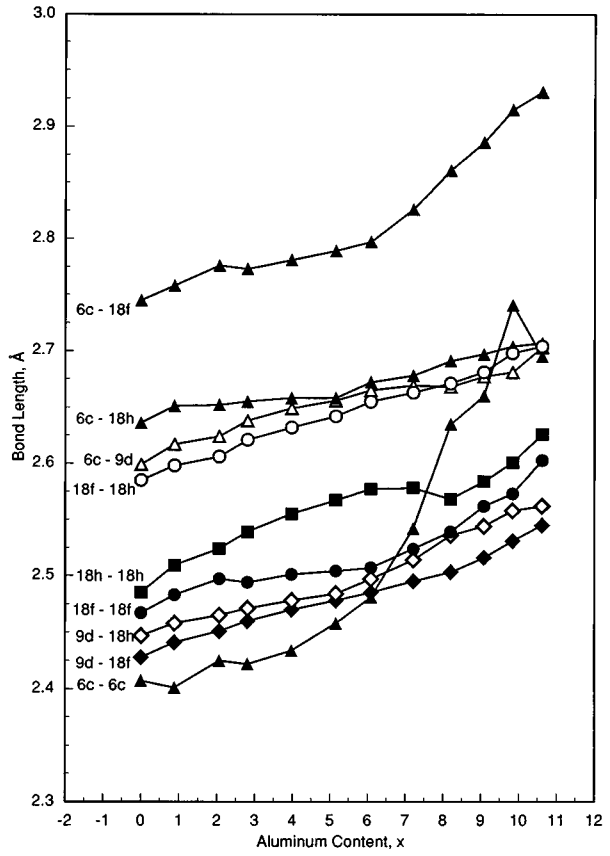

FIG. 5. The iron–iron bond lengths in the $Ce_2Fe_{17-x}Al_x$ solid solutions as a function of aluminum content.

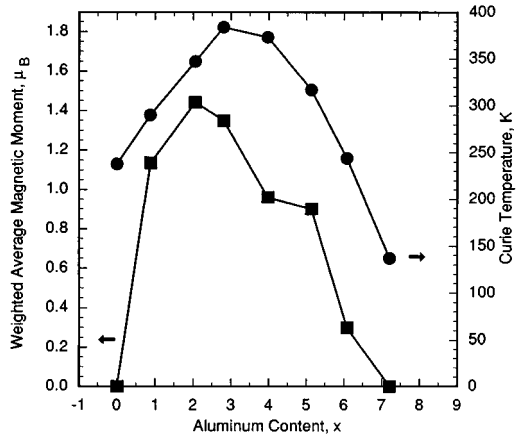

FIG. 6. The neutron diffraction derived weighted average magnetic moment and Curie temperature for the $Ce_2Fe_{17-x}Al_x$ solid solutions as a function of aluminum content.

that observed[12,13] for $Nd_2Fe_{17-x}Al_x$ and $Tb_2Fe_{17-x}Al_x$. Because aluminum has a larger metallic radius than iron, it avoids, at all x values studied, the 9d site, the site with the smallest Wigner–Seitz cell volume.[11,15–17] For $x \leqslant 6$ aluminum shows a marked preference for the 18h site instead of the 6c site, even though the 6c site has the largest cell volume. However, it should be noted that the 18h site is the only site with as many as three cerium near neighbors. If the aluminum atoms prefer to associate with the rare earth, as has been found for Si, this would account for the high aluminum occupancy of this site. Aluminum shows an almost equal preference for the 6c and 18f site for $x \leqslant 6$, and for the higher values of x, aluminum shows a preference for the 6c site. The structural basis for the site occupancy pattern has been previously discussed[12,18] in detail for $Nd_2Fe_{17-x}Al_x$ and $Tb_2Fe_{17-x}Ga_x$.

The neutron diffraction results indicate that, as shown in Fig. 6, the site averaged room temperature iron magnetic moments in the $Ce_2Fe_{17-x}Al_x$ solid solutions increase dramatically from $x=0$ to 2 and then decrease slowly from $x=2$ to 6 and reach zero for $x>6$. The small moments found for $Ce_2Fe_{10.92}Al_{6.08}$ are within the uncertainty, one sigma, of zero and have a minimal effect on the agreement factors. However, statistical tests do not confirm a nonzero value. In contrast, the refinement for $Ce_2Fe_{16.12}Al_{0.88}$ yields larger moments and the agreement factors are slightly, but statistically, better than with zero moments even when all the remaining parameters are adjusted. Because the Curie temperature is very close to room temperature for this compound, the difference between the neutron diffraction results and the Mössbauer spectral results may reflect a difference in the ambient temperature in the two different laboratories. However, it should be noted that the calculated magnetic scattering intensity for $Ce_2Fe_{16.12}Al_{0.88}$ is only 1.27% of the total diffracted intensity, and thus is approaching the limit of detectibility in a ferromagnetic phase in which the nuclear and magnetic peaks are coincident. The variation in the ferromagnetic moments, all of which lie in the basal plane, agrees well, as expected, with the variation in the Curie temperature (see Fig. 6).

TABLE II. The Curie temperatures, 5.0 K magnetic moments, and exchange coupling constants for $Ce_2Fe_{17-x}Al_x$.

x	T_C, K[a]	μ_s/fu, μ_B	μ_{Fe}, μ_B	J_{FeFe}/k_B, K
0	238	32.8	1.93	19
0.88	290	28.5	1.76	27
2.06	347	26	1.74	36
2.81	384	23	1.61	47
3.98	373	21	1.60	50
5.14	317	18.5	1.55	49
6.08	244	15.5	1.40	47
7.21	137	10.5	1.07	43

[a]Values obtained from Ref. 7.

In order to obtain more information on the exchange interactions between the unpaired spins of the magnetic constituents in $Ce_2Fe_{17-x}Al_x$, the mean values of the exchange coupling constant, J_{FeFe}, have been calculated, as discussed elsewhere,[1,9] through a mean-field analysis of the Curie temperatures and the saturation magnetizations. Table II lists the average iron moments derived from the saturation magnetization values. The lower average 5 K iron magnetic moments of $\sim$1.9 to 1.0 μ_B in $Ce_2Fe_{17-x}Al_x$, as compared to $\sim$2.3 μ_B in α-iron, result from the mixing of the $3d$ band of iron with the valence band of aluminum. This mixing leads to an increase in the bandwidth of the $3d$ band, an increase which lowers the iron magnetic moment as a result of the reduced exchange splitting of the $3d$ band. The substitution of aluminum for iron in Ce_2Fe_{17} modifies the density of states at the Fermi level and the position of the Fermi level in the conduction band. First-principles calculations,[19] with an orthogonalized linear combination of atomic orbitals in the local spin density approximation, on $Nd_2Fe_{17-x}Al_x$ show that the aluminum $3p$ states are $\sim$4.5 eV below the Fermi level and hence mix with the low-lying majority spin states of iron. These calculations also show that the conduction bandwidth is not strongly modified by lattice expansion, that the exchange splitting between the majority and minority spin bands increases only slightly with increasing aluminum content, and that the total area below the Fermi level decreases because of the reduced number of electrons with increasing aluminum content. Thus, it is reasonable to expect a similar band structure for the $Ce_2Fe_{17-x}Al_x$ solid solutions as the aluminum substitution pattern is similar[12] to that in $Nd_2Fe_{17-x}Al_x$. Electrical resistivity measurements on $Ce_2Fe_{17-x}Al_x$ for $x=0.0$, 0.2, 0.4, 0.88, and 2.06, indicate that the resistivity at a given temperature increases with x, in agreement with the decreasing number of electrons in the conduction band and their localization on the aluminum atoms as revealed by the band structure calculations.[19,20]

In the absence of band structure calculations on the $R_2Fe_{17-x}Si_x$ solid solutions, only a very qualitative comparison of the electronic structure of the $Ce_2Fe_{17-x}Si_x$ and $Ce_2Fe_{17-x}Al_x$ solid solutions is possible. Because of the lattice contraction observed[9] in the $Ce_2Fe_{17-x}Si_x$ solid solutions, the conduction bandwidth is expected to be slightly larger than in the $Ce_2Fe_{17-x}Al_x$ solid solutions. Because silicon has one more electron than aluminum, the number of electrons below the Fermi level is larger in $Ce_2Fe_{17-x}Si_x$ than in $Ce_2Fe_{17-x}Al_x$. However, electrical resistivity measurements[20] show that the resistivities of the $Ce_2Fe_{17-x}Si_x$ solid solutions are higher than those of the corresponding $Ce_2Fe_{17-x}Al_x$ solid solutions and, hence, the electrons are more localized on the silicon atoms. All of these combined effects lead to an average iron magnetic moment which is 0.2 μ_B larger in the $Ce_2Fe_{17-x}Si_x$ than in $Ce_2Fe_{17-x}Al_x$ solid solutions.

The temperature dependence of the magnetization of the $Ce_2Fe_{17-x}Al_x$ solid solutions has been reported earlier.[7] The substitution of aluminum for iron leads to normal ferromagnetism for $x \leqslant 7.21$ and a maximum Curie temperature of 384 K for $x=2.81$. The lower Curie temperatures of $Ce_2Fe_{17-x}Al_x$, as compared[12,13] to those of $Nd_2Fe_{17-x}Al_x$ and $Tb_2Fe_{17-x}Al_x$, may be due to the absence of rare-earth–iron exchange coupling and to the lower average moment carried by the iron in $Ce_2Fe_{17-x}Al_x$ and, hence, the lower iron–iron exchange coupling (see Table II). The absence of a magnetic moment on cerium indicates that the cerium–iron exchange does not play any role in determining the Curie temperature, in contrast to the case of the heavier rare-earth solid solutions. For the higher aluminum concentrations of $x=8.20$, 9.84, and 10.62 the magnetization curves show sharp cusps,[7] suggesting the onset of spin-glass ordering at about 48, 32, and 19 K, respectively. This spin-glass ordering, or better cluster glass ordering, arises as a consequence of aluminum concentration fluctuations.[21]

The Mössbauer spectra of the $Ce_2Fe_{17-x}Al_x$ solid solutions have been measured at 85 and 295 K and reveal details of the influence of aluminum substitution on the magnetic properties of Ce_2Fe_{17}. The Mössbauer spectra reported herein have been fit with a model in which the magnetization and hyperfine field lie in the basal plane of the unit cell. Under the combined effect of the magnetic dipole and electric quadrupole interactions, the Mössbauer spectra of $Ce_2Fe_{17-x}Al_x$ are composed of seven magnetic components representing the $6c$, $9d_6$, $9d_3$, $18f_{12}$, $18f_6$, $18h_{12}$, and $18h_6$ magnetically distinct iron sites.[11] The difference in the hyperfine fields of the crystallographically equivalent, but magnetically inequivalent, iron sites results from the anisotropic dipolar and orbital contributions to the hyperfine field.[22] Because the near-neighbor environment of a particular iron site is influenced by the presence of aluminum, a distribution of the hyperfine parameters results at each iron site. By using the aluminum occupancy obtained from the neutron diffraction results listed in Table I, the binomial distribution of the aluminum near neighbors of a specific iron site may be calculated. Thus in the Mössbauer spectral fits, the sextet corresponding to a given crystallographically and magnetically unique iron site is replaced by several sextets, each resulting from an iron atom on the site having a different number of aluminum near neighbors. The hyperfine field is given by $H(x,n)=H_{max}(x)-n\Delta H(x)$, where H_{max} is the hyperfine field at an iron site which has zero aluminum near neighbors, and the decremental field, ΔH, is the decrease in the hyperfine field when one near-neighbor iron is replaced by aluminum. In all cases, the distributions of quadrupole interactions and isomer shifts were ignored and each spectrum was fit with a single linewidth for all components. The linewidth is

TABLE III. Mössbauer spectral parameters for $Ce_2Fe_{17-x}Al_x$ obtained at 85 K.

Parameter	x	Site							Wt. avg.	Γ, mm/s
		$6c$	$9d_6$	$9d_3$	$18f_{12}$	$18f_6$	$18h_{12}$	$18h_6$		
H_{max} (kOe)	0.20	299	245	236	226	258	225	211	232	
	0.40	304	246	238	234	264	231	217	238	
	0.60	308	250	245	237	269	233	218	241	
	0.80	313	249	245	234	270	232	216	240	
	0.88	308	245	236	236	271	236	204	239	
	2.06	303	248	243	227	270	228	196	237	
	2.81	290	237	225	216	256	213	179	220	
	3.98	276	221	224	200	237	201	159	204	
	5.15	249	199	187	178	210	187	139	184	
	7.21	141	104	83	55	124	77	27	78	
ΔH (kOe)	0.20	16	11	10	13	14	19	17	15	
	0.40	17	11	10	13	14	19	17	15	
	0.60	17	11	10	13	14	19	17	15	
	0.80	17	11	10	13	14	19	17	15	
	0.88	16	11	10	13	14	19	17	14	
	2.06	15	11	10	12	12	17	15	13	
	2.81	14	11	10	12	12	17	14	13	
	3.98	11	10	10	12	12	17	12	12	
	5.15	11	10	10	11	11	16	12	12	
	7.21	9	9	9	10	10	15	11	10	
δ (mm/s)[a]	0.20	0.20	−0.05	−0.05	0.00	0.00	−0.01	−0.01	0.00	0.30
	0.40	0.20	−0.05	−0.05	0.00	0.00	−0.01	−0.01	0.00	0.37
	0.60	0.21	−0.05	−0.05	0.02	0.02	−0.01	−0.01	0.01	0.36
	0.80	0.20	−0.04	−0.04	0.03	0.03	−0.01	−0.01	0.02	0.36
	0.88	0.20	−0.03	−0.03	0.04	0.04	0.00	0.00	0.03	0.36
	2.06	0.21	−0.02	−0.02	0.04	0.04	0.02	0.02	0.04	0.36
	2.81	0.23	−0.01	−0.01	0.07	0.07	0.04	0.04	0.06	0.36
	3.98	0.22	0.02	0.02	0.09	0.09	0.06	0.06	0.08	0.44
	5.15	0.23	0.02	0.02	0.10	0.10	0.07	0.07	0.09	0.44
	7.21	0.30	0.08	0.08	0.20	0.20	0.15	0.15	0.15	0.44
	10.62	0.10	0.19	⋯	0.12	⋯	0.23	⋯	0.20	0.32
QS (mm/s)	b	0.09	0.04	0.49	0.40	−0.06	−0.40	0.47	⋯	
ΔE_Q (mm/s)	10.62	0.48	0.45	⋯	0.29	⋯	0.24	⋯	0.34	

[a]Relative to α-iron foil at 295 K.
[b]The same values were used for all x values between 0.2 and 7.21.

typically larger than the ~0.24 mm/s observed in the α-iron foil calibration spectrum, an increase which probably results from the distributions of the quadrupole interaction and isomer shift which were neglected in our fits.

In the Mössbauer spectral fits, each of the seven magnetically inequivalent iron sites is characterized by four hyperfine parameters, the isomer shift, δ, the quadrupole shift, QS, the maximum hyperfine field, H_{max}, and the decremental field, ΔH. Hence there is a maximum of 28 adjustable hyperfine parameters. However, the isomer shifts of the crystallographically equivalent iron sites are constrained to be equal, and this constraint reduces the number of adjustable parameters to 25. In addition, the seven quadrupole shift values were obtained from fits with seven broadened sextets and subsequently constrained to these values in the binomial distribution fits. In addition, a linewidth and a total absorption area were fit, bringing the total number of adjustable parameters in the binomial distribution fits to 20. A doublet with an area of ~2%–5% of the total spectral absorption area was included in all the Mössbauer spectral fits. This doublet has a temperature independent quadrupole splitting of ~1.0 mm/s and an isomer shift of ~−0.08 mm/s at 85 K and ~−0.10 mm/s at 295 K.

The hyperfine parameters resulting from the distribution fits of the Mössbauer spectra of the $Ce_2Fe_{17-x}Al_x$ solid solutions, measured at 85 and 295 K, are given in Tables III and IV, and some of the resulting spectral fits are shown in Figs. 7 and 8. The 85 K weighted average maximum hyperfine field, H_{max} (see Table III) reaches a maximum of 241 kOe for $Ce_2Fe_{16.4}Al_{0.6}$ and decreases by ~25 kOe per aluminum for higher values of x, a decrease which is due to the dilution of the iron magnetic moment by aluminum. The $Ce_2Fe_{17-x}Al_x$ samples with x equal to 0.0, 0.2, 0.4, 0.6, 0.8, 0.88, 7.21, and 10.62 are paramagnetic at 295 K and $H(x,n)$ is zero and, as a result, these points are omitted from Fig. 9, a figure which shows that the maximum in H_{max} at 295 K occurs for $x=2.81$, the same aluminum content which yields the maximum Curie temperature. As is usually observed in the R_2Fe_{17} compounds,[11] the maximum hyperfine fields in $Ce_2Fe_{17-x}Al_x$ (see Figs. 9 and 10) decrease in the order $H_{max}(6c)>H_{max}(9d)>H_{max}(18f)>H_{max}(18h)$, the order of the decreasing number of iron near neighbors and the order of the neutron-diffraction determined magnetic moments observed in $Ce_2Fe_{14.94}Al_{2.06}$ (see Table I and Fig. 4).

The presence of aluminum in the $Ce_2Fe_{17-x}Al_x$ lattice increases all the magnetically distinct iron hyperfine fields

TABLE IV. Mössbauer spectral parameters for $Ce_2Fe_{17-x}Al_x$ obtained at 295 K.

Parameter	x	Site								
		$6c$	$9d_6$	$9d_3$	$18f_{12}$	$18f_6$	$18h_{12}$	$18h_6$	Wt. avg.	Γ, mm/s
H_{max} (kOe)	2.06	186	136	132	135	160	137	70	135	
	2.81	199	162	162	141	171	136	123	146	
	3.98	189	150	128	133	167	116	92	131	
	5.15	113	104	82	61	96	75	66	80	
ΔH (kOe)	2.06	14	11	10	13	15	16	15	14	
	2.81	13	10	9	13	13	16	15	12	
	3.98	12	9	8	11	12	13	13	10	
	5.15	11	8	7	13	11	13	12	11	
δ (mm/s)[a]	0.20	−0.11	−0.22	⋯	−0.12	⋯	−0.14	⋯	−0.15	0.26
	0.40	−0.10	−0.20	⋯	−0.12	⋯	−0.13	⋯	−0.14	0.26
	0.60	−0.10	−0.20	⋯	−0.12	⋯	−0.13	⋯	−0.14	0.26
	0.80	−0.10	−0.20	⋯	−0.12	⋯	−0.13	⋯	−0.14	0.26
	0.88	−0.09	−0.20	⋯	−0.11	⋯	−0.13	⋯	−0.13	0.26
	2.06	−0.01	−0.20	−0.20	−0.05	−0.05	−0.16	−0.16	−0.10	0.32
	2.81	0.02	−0.18	−0.18	−0.03	−0.03	−0.14	−0.14	−0.08	0.36
	3.98	0.10	−0.15	−0.15	0.00	0.00	−0.07	−0.07	−0.05	0.44
	5.15	0.10	−0.13	−0.13	0.08	0.08	−0.10	−0.10	−0.02	0.44
	7.21	0.10	−0.04	⋯	0.07	⋯	0.05	⋯	0.04	0.26
	10.62	0.10	0.06	⋯	0.08	⋯	0.10	⋯	0.08	0.29
QS (mm/s)	b	0.09	0.04	0.49	0.40	−0.06	−0.40	0.47	⋯	
ΔE_Q (mm/s)	0.20	0.72	0.69	⋯	0.68	⋯	0.38	⋯	0.60	
	0.40	0.73	0.70	⋯	0.70	⋯	0.36	⋯	0.60	
	0.60	0.74	0.70	⋯	0.68	⋯	0.37	⋯	0.60	
	0.80	0.73	0.70	⋯	0.67	⋯	0.38	⋯	0.60	
	0.88	0.73	0.71	⋯	0.67	⋯	0.37	⋯	0.60	
	7.21	0.78	0.67	⋯	0.61	⋯	0.27	⋯	0.52	
	10.62	0.48	0.40	⋯	0.36	⋯	0.20	⋯	0.32	

[a]Relative to α-iron foil at 295 K.
[b]The same values were used for all x values between 2.06 and 5.15.

for $x<1$ and decreases them for $x>1$ at 85 K (see Fig. 10). The weighted average H_{max} at 85 K for $Ce_2Fe_{17-x}Al_x$ is lower at all x values studied than for $R_2Fe_{17-x}M_x$, where R is Nd or Tb and M is Al or Ga.[12,13,18] Similarly, the range of magnetic moments at 5 K (see Table II) in $Ce_2Fe_{17-x}Al_x$ is lower than the range measured[12,13] by neutron diffraction at 10 K for the $Nd_2Fe_{17-x}Al_x$ and $Tb_2Fe_{17-x}Al_x$ solid solutions. The smaller fields observed in $Ce_2Fe_{17-x}Al_x$ may be related to the virtually zero magnetic moment[23] of cerium as compared to the rather large magnetic moments[12,13] of neodymium and terbium in $Nd_2Fe_{17-x}Al_x$ and $Tb_2Fe_{17-x}Al_x$. The weighted average H_{max} of $Ce_2Fe_{17-x}Al_x$ decreases by 11 kOe per aluminum at 85 K between x values of 0.88 and 3.98. This decrease is expected because of the dilution of the magnetic moments resulting from the substitution of iron by aluminum. However, this decrease is larger than the decrease of ~6 kOe per silicon observed[9] in the $Ce_2Fe_{17-x}Si_x$ solid solutions between x values of 1 and 3. The larger decrease in H_{max} in the $Ce_2Fe_{17-x}Al_x$ solid solutions reflects the equally large decrease of the average iron moment, a decrease which reduces the on-site iron moment and the concomitant core polarization.

The decremental fields, ΔH, which are shown at 85 K as a function of aluminum content in Fig. 11, decrease by 1.0 kOe per aluminum both at 85 and 295 K. A similar decrease has been observed[12,24] for $Nd_2Fe_{17-x}Al_x$ and $Tb_2Fe_{17-x}Al_x$. This decrease in ΔH indicates that, at low aluminum content, the near-neighbor aluminum atoms reduce the hyperfine field, but at higher concentrations of aluminum the decrease becomes smaller as the more distant aluminum atoms actually increase the hyperfine field. This behavior may be interpreted as arising from the spatial oscillation of the conduction electron polarization resulting from the Ruderman–Kittel–Kasuya–Yosida (RKKY)-type polarization mechanism.[25–29] This mechanism produces a spatial oscillation in the 4 s conduction electron spin density extending from neighboring solute atoms to the iron, thus changing the Fermi contact contribution to the iron hyperfine field. The decrease in ΔH in $R_2Fe_{17-x}Al_x$, where R is Ce, Nd, and Tb, is in contrast to the constant value of ΔH with x observed[9] for the $Ce_2Fe_{17-x}Si_x$ solid solutions, and shows the presence of an enhanced perturbation by aluminum on the long-range magnetic interactions in the $R_2Fe_{17-x}Al_x$ solid solutions. The strength of the RKKY interaction is distance dependent and varies as the lattice expands with aluminum substitution in $Ce_2Fe_{17-x}Al_x$.

In all the Mössbauer spectral fits the isomer shifts of the crystallographically equivalent iron sites in $Ce_2Fe_{17-x}Al_x$ were constrained to be equal. As shown in Fig. 12, the four individual isomer shifts increase with increasing x and the weighted average isomer shift increases by 0.016 mm/s per aluminum at 85 K. At 295 K the equivalent weighted average increase is 0.029 mm/s. The increase in the isomer shift with aluminum content indicates that there is a decrease in the s-electron density at the iron nuclei. The increase in the isomer shift with aluminum content results from the $3d$ band

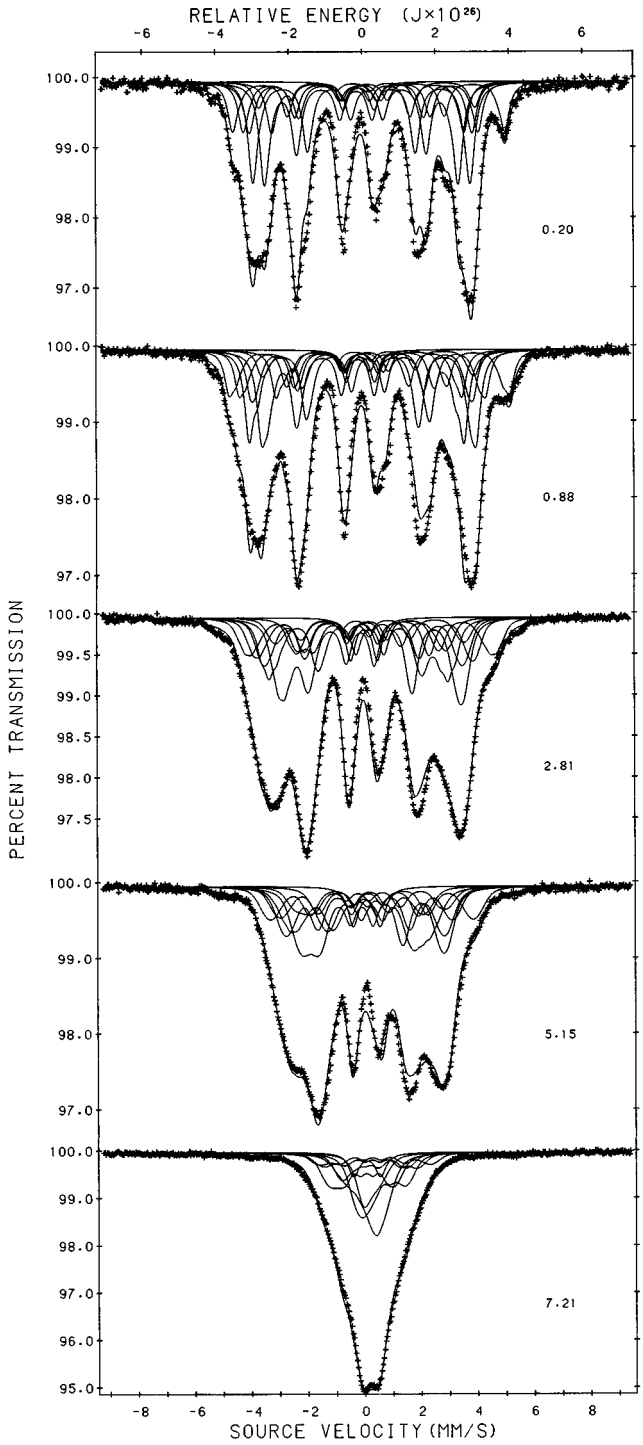

FIG. 7. The Mössbauer spectra of the $Ce_2Fe_{17-x}Al_x$ solid solutions obtained at 85 K.

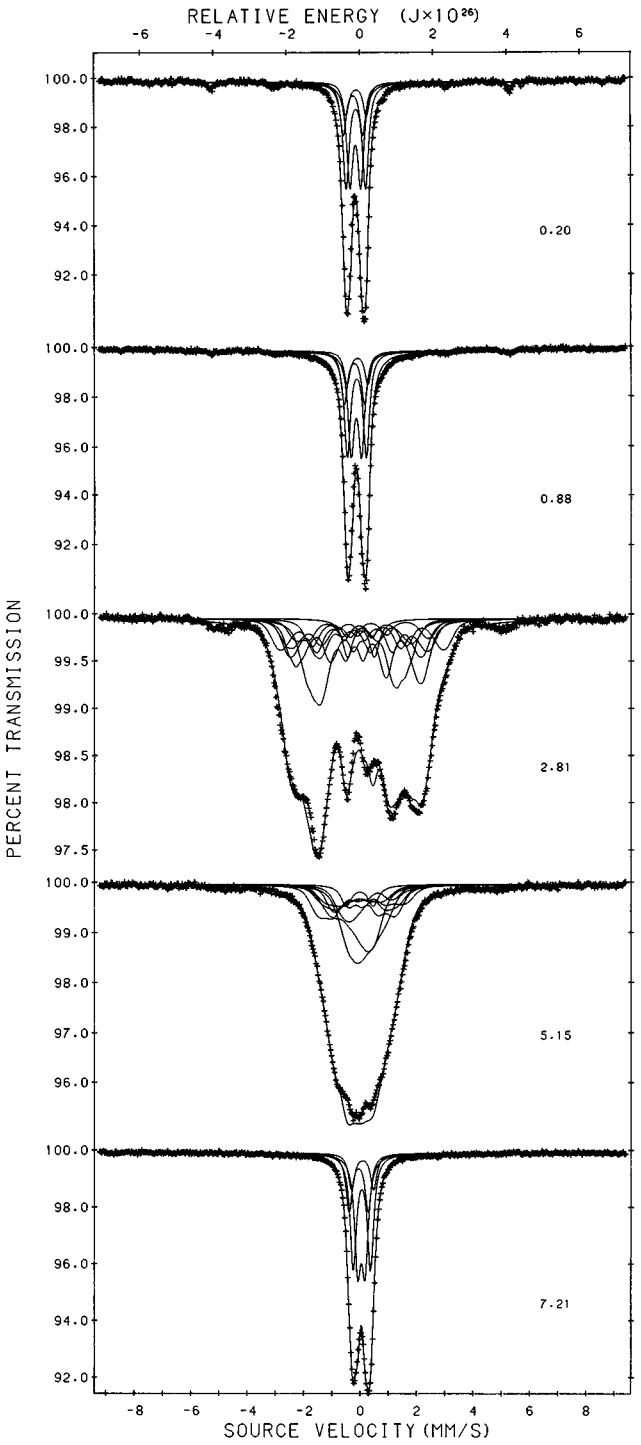

FIG. 8. The Mössbauer spectra of the $Ce_2Fe_{17-x}Al_x$ solid solutions obtained at 295 K.

mixing with the aluminum $3p$ valence band, a consequent $3d-4s$ intratomic iron electronic redistribution,[30–32] and an additional screening of the $4s$ electrons. The observed increases in the weighted average isomer shifts are much smaller than the increases expected from the calculated[19] transfer of 1.8 electrons from iron to an aluminum near neighbor. This reduction indicates that some of the assumptions made in the calculations may be over simplified. The isomer shift[12] of Nd_2Fe_{17} is 0.061 mm/s at 85 K. In comparison, the 85 K isomer shift of Ce_2Fe_{17} is 0.016 mm/s, as calculated from the extrapolated values of the isomer shifts in the $Ce_2Fe_{17-x}Al_x$ solid solutions as a function of their unit cell volumes. The greater value of the isomer shift in Nd_2Fe_{17}, which has a unit cell volume ~3% larger than that of Ce_2Fe_{17}, demonstrates the sensitivity of the isomer shift to the unit cell volume.

The second order Doppler shifts indicate that the average effective recoil mass of iron in the $Ce_2Fe_{17-x}Al_x$ solid solu-

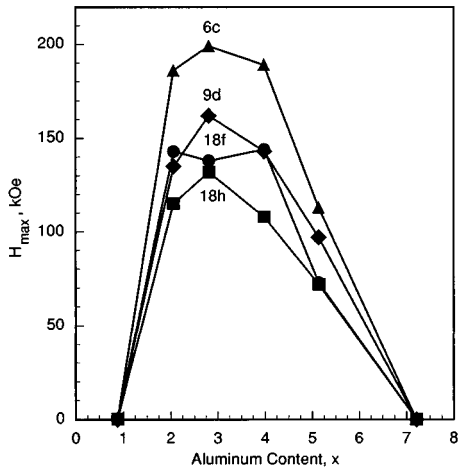

FIG. 9. The maximum hyperfine fields at 295 K for the four iron sites in the $Ce_2Fe_{17-x}Al_x$ solid solutions as a function of aluminum content.

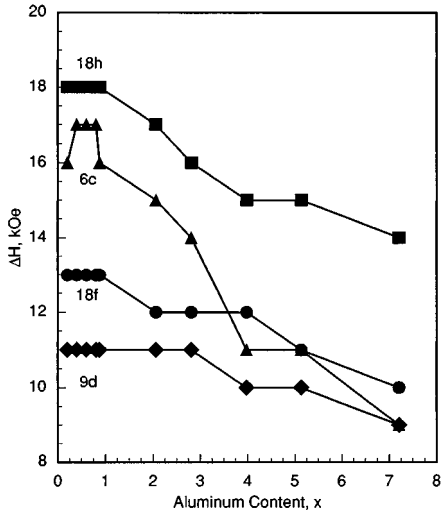

FIG. 11. The decremental hyperfine field, ΔH, at 85 K for the four iron sites in the $Ce_2Fe_{17-x}Al_x$ solid solutions as a function of aluminum content.

tions range from ~65 to 80 g/mol, generally increasing with increasing aluminum content.[33] These values are somewhat lower than the values[9] of ~80–90 g/mol found for $Ce_2Fe_{17-x}Si_x$, indicating an increased covalency of the iron–silicon bonding over that of the iron–aluminum bonding, an increase which agrees with the relative bond distances.

IV. DISCUSSION

The results obtained in this investigation are interesting because they help to elucidate the origin of the Curie temperature enhancement observed in several series of $R_2Fe_{17-x}M_x$ compounds, where M is Al, Ga, or Si.

The Curie temperatures of the $R_2Fe_{17-x}M_x$ solid solutions, where R is Ce, Nd, or Tb, and M is Al, Ga, or Si reach a maximum[9,12,18,24] for x values of ~3–4. The lower iron magnetic moments in $Ce_2Fe_{14}Al_3$ give rise to the lower Curie temperature of $Ce_2Fe_{14}Al_3$ as compared to $Ce_2Fe_{14}Si_3$. A comparison of the unit cell volumes of $Ce_2Fe_{17-x}Al_x$ and $Ce_2Fe_{17-x}Si_x$ (see Fig. 2) indicates, in agreement with the above conclusion, that the volume of the unit cell does not play a major role in determining the Curie temperature because an increase in the Curie temperature of $Ce_2Fe_{17-x}Si_x$ occurs with increasing x, even though its unit cell contracts.[9] The expansion of the c axis in $R_2Fe_{17-x}M_x$, where R is cerium and neodymium and M is aluminum[12] or silicon,[9,34] seems at first to be one of the factors responsible for the increased Curie temperature of these compounds; however, the rate of expansion of the c axes of ~0.02 Å per silicon in $Ce_2Fe_{17-x}Si_x$ is smaller than the rate of expansion of ~0.05 Å per aluminum in $Ce_2Fe_{17-x}Al_x$. Thus, the different degrees of mixing of the iron $3d$ band with the solute valence

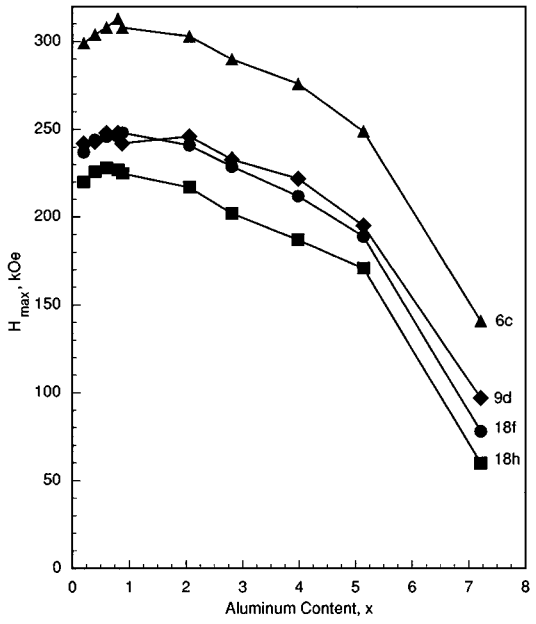

FIG. 10. The maximum hyperfine fields at 85 K for the four iron sites in the $Ce_2Fe_{17-x}Al_x$ solid solutions as a function of aluminum content.

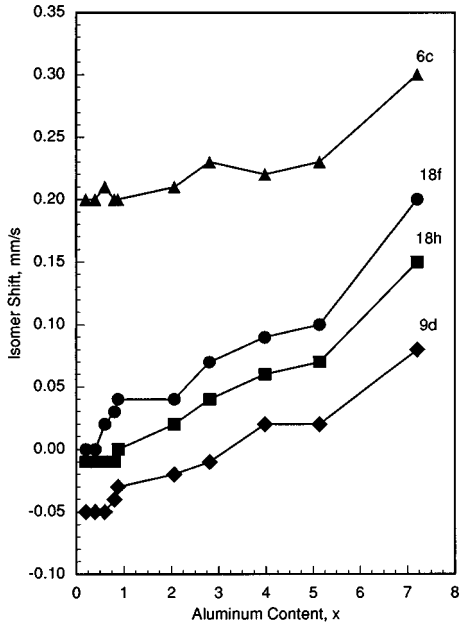

FIG. 12. The isomer shift at 85 K for the four iron sites in the $Ce_2Fe_{17-x}Al_x$ solid solutions as a function of aluminum content.

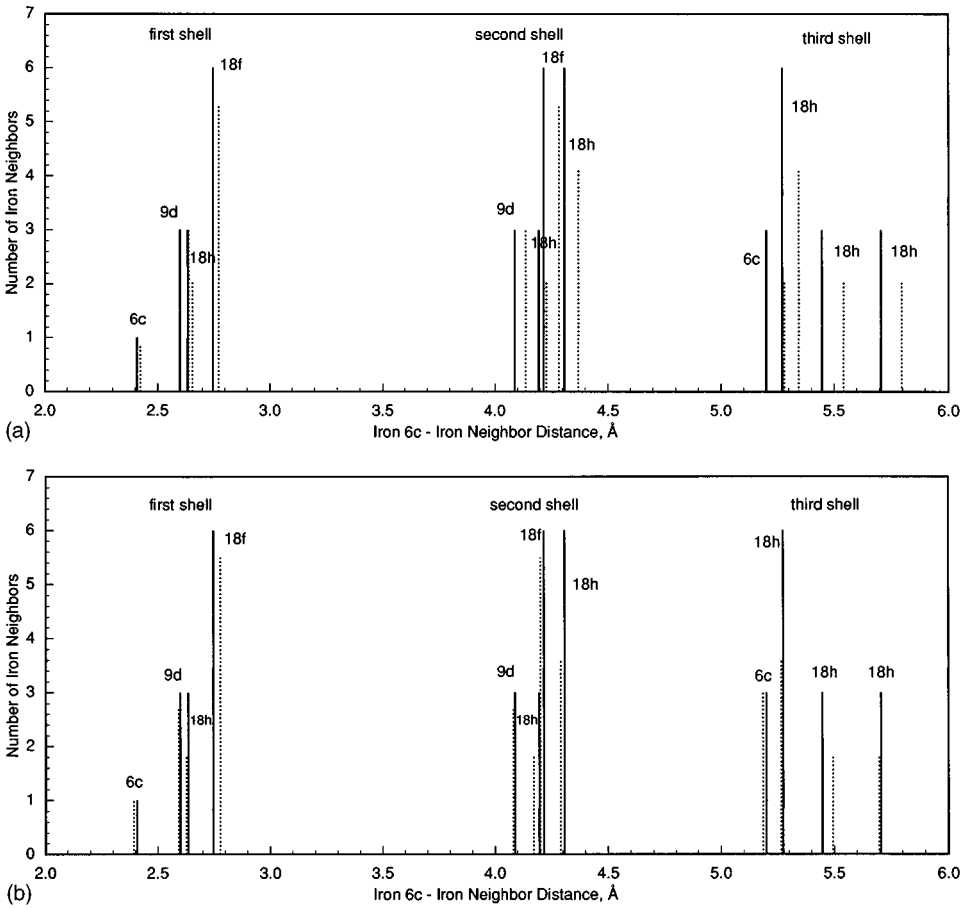

FIG. 13. A plot of the number of iron neighbors for the iron 6*c* site as a function of distance in Ce_2Fe_{17}, solid lines and $Ce_2Fe_{14}Al_3$, dashed lines, A, and $Ce_2Fe_{14}Si_3$, dashed lines, B.

band is most likely responsible for the difference in the Curie temperatures of the $Ce_2Fe_{17-x}Al_x$ and $Ce_2Fe_{17-x}Si_x$ solid solutions.

The decrease in ΔH with aluminum content results from the RKKY conduction electron polarization arising from iron atoms at a greater distance than the nearest neighbor and involving mainly the iron 4*s* conduction band electrons as modified by the presence of aluminum. The decrease in ΔH with increasing aluminum content, indicating the presence of a long-range magnetic influence of aluminum in $Ce_2Fe_{17-x}Al_x$, is apparently reduced in $Ce_2Fe_{17-x}Si_x$, in which ΔH is independent[9] of silicon content. In an earlier article[12] we have discussed the hyperfine field behavior in the $Nd_2Fe_{17-x}Al_x$ solid solutions in terms of the variation of the distance to and the number of iron atoms in the various near-neighbor shells. Because the decrease in ΔH with aluminum content is the largest for the 6*c* site, as shown in Fig. 11 and Table III, we compare the same variations for the 6*c* site in Ce_2Fe_{17} and $Ce_2Fe_{14}Al_3$ in Fig. 13(a) and for Ce_2Fe_{17} and $Ce_2Fe_{14}Si_3$ in Fig. 13(b). Only the iron atoms have been included in Fig. 13 because, presumably, the cerium and aluminum do not contribute to conduction electron polarization. It is clear that opposite changes are observed in the two parts of Fig. 13. It seems unlikely to us that changes in the first near-neighbor shell, between 2.4 and 2.8 Å, or in the second shell, between 4.1 and 4.3 Å, can account for the difference between $Ce_2Fe_{17-x}Al_x$ and $Ce_2Fe_{17-x}Si_x$, although changes in the third shell, between 5.2 and 5.7 Å, could be more important. From Fig. 13(a) it is clear that the center of gravity of the third shell 6*c* bond distances increase in going from Ce_2Fe_{17} to $Ce_2Fe_{14}Al_3$, whereas little analogous shift is observed in going from Ce_2Fe_{17} to $Ce_2Fe_{14}Si_3$ [see Fig. 13(b)].

The increase in the isomer shifts observed in $Ce_2Fe_{17-x}Al_x$ and $Ce_2Fe_{17-x}Si_x$ can be decomposed[35,36] into volume and chemical contributions. The volume term can be calculated from the variation of the logarithm of the volume with x in both $Ce_2Fe_{17-x}Al_x$ and $Ce_2Fe_{17-x}Si_x$, for $0 \leqslant x < 3$ and the variation of the weighted average isomer shift with the logarithm of the volume, $+1.95$ mm/s, observed[36] for Gd_2Fe_{17} under high pressure. From the increase of the weighted average isomer shifts reported here for $Ce_2Fe_{17-x}Al_x$ and observed[9] for $Ce_2Fe_{17-x}Si_x$, the chemical contribution can be estimated to be -0.004 mm/s per aluminum and $+0.028$ mm/s per silicon, respectively. This difference indicates that different mechanisms are responsible for the observed increase in the isomer shift in aluminum and silicon substituted Ce_2Fe_{17} compounds. Any change in the *s*-electron charge density at the nucleus brings about a change in the isomer shift. In $Ce_2Fe_{17-x}Al_x$ this occurs because of an increase in the 3*d* electron density resulting from the band mixing with the aluminum valence band, producing

a lower 4*s* charge density at the nucleus and resulting in an increased isomer shift. In contrast, in the case of $Ce_2Fe_{17-x}Si_x$, direct mixing of 4*s* conduction electrons with the valence band of silicon results in the charge redistribution in the 4*s* band electrons such that *s*-electron charge density is reduced at the nucleus, thus increasing the isomer shift.[37]

ACKNOWLEDGMENTS

The authors acknowledge, with thanks, NATO for Cooperative Scientific Research Grant No. 92-1160, the Division of Materials Research of the U.S. National Science Foundation, for Grants Nos. DMR-92142711 and DMR-9305782, and the Ministère de la Communauté Française of Belgium for Grant No. A.R.C. 94/99-175. D.P.M. would like to acknowledge the stimulating support of L. J. de Jongh and to thank the Stitching voor Fundamenteel Onderzoek der Materie, which is financially supported by the Nederlandse Organisatie voor Wetenschappelijk Onderzoek.

[1] K. H. J. Buschow, Rep. Prog. Phys. **40**, 1179 (1977).
[2] D. Givord and R. Lemaire, IEEE Trans. Magn. **MAG-10**, 109 (1974).
[3] J. M. D. Coey and H. Sun, J. Magn. Magn. Mater. **87**, L251 (1990).
[4] M. Guermain, A. Beginge, K. Yvon, and J. Muller, Solid State Commun. **64**, 639 (1987).
[5] Y. P. Hong, R. Y. Rawanscki, F. R. de Boer, T. H. Jacobs, and K. H. J. Buschow, J. Magn. Magn. Mater. **83**, 143 (1990).
[6] F. Weitzer, K. Hieble, and P. Rogl, J. Appl. Phys. **65**, 4963 (1989).
[7] D. P. Middleton and K. H. J. Buschow, J. Alloys Comp. **203**, 2117 (1994).
[8] T. W. Capehart, R. K. Mishra, G. P. Meisner, C. D. Fuerst, and J. F. Herbst, Appl. Phys. Lett. **63**, 3642 (1993).
[9] D. P. Middleton, S. R. Mishra, G. J. Long, O. A. Pringle, Z. Hu, W. B. Yelon, F. Grandjean, and K. H. J. Buschow, J. Appl. Phys. **78**, 5568 (1995).
[10] FULLPROF Rietveld refinement code written by J. Rodriguez-Carjaval, Institut Laue Langevin, Grenoble, France.
[11] F. Grandjean and G. J. Long, in *Interstitial Intermetallic Alloys*, edited by F. Grandjean, G. J. Long, and K. H. J. Buschow (Kluwer, Dordrecht, 1995), p. 463.
[12] G. J. Long, G. K. Marasinghe, S. Mishra, O. A. Pringle, Z. Hu, W. B. Yelon, D. P. Middleton, K. H. J. Buschow, and F. Grandjean, J. Appl. Phys. **76**, 5383 (1994).
[13] G. K. Marasinghe, S. Mishra, O. A. Pringle, G. J. Long, Z. Hu, W. B. Yelon, F. Grandjean, D. P. Middleton, and K. H. J. Buschow, J. Appl. Phys. **76**, 6731 (1994).
[14] S. Miraglia, J. L. Soubeyroux, C. Kolbeck, O. Isnard, and D. Fruchart, J. Less-Common Met. **171**, 504 (1993).
[15] G. J. Long, O. A. Pringle, F. Grandjean, W. B. Yelon, and K. H. J. Buschow, J. Appl. Phys. **74**, 504 (1994).
[16] G. J. Long, O. A. Pringle, F. Grandjean, and K. H. J. Buschow, J. Appl. Phys. **72**, 4845 (1992).
[17] L. Gelato, J. Appl. Crystallogr. **14**, 141 (1981).
[18] Z. Hu, W. B. Yelon, S. Mishra, G. J. Long, O. A. Pringle, D. P. Middleton, K. H. J. Buschow, and F. Grandjean, J. Appl. Phys. **76**, 443 (1994).
[19] M. Z. Huang and W. Y. Ching, J. Appl. Phys. **76**, 7046 (1994).
[20] D. Vandormael, F. Grandjean, H. Bougrine, M. Ausloos, D. P. Middleton, K. H. J. Buschow, and G. J. Long (unpublished).
[21] J. A. Mydosh and G. J. Niewenhuys, in *Ferromagnetic Materials*, edited by E. P. Wohlfarth (North-Holland, Amsterdam, 1980), Vol. 1, p. 71.
[22] M. Kawakami, T. Hihara, Y. Koi, and T. Wakiyama, J. Phys. Soc. Jpn. **33**, 1591 (1972).
[23] O. Isnard, S. Miraglia, D. Fruchart, C. Giorgetti, S. Pizzini, E. Dartyge, G. Krill, and J. P. Kappler, Phys. Rev. B **49**, 15692 (1994).
[24] S. R. Mishra, G. J. Long, O. A. Pringle, Z. Hu, W. B. Yelon, D. P. Middleton, K. H. J. Buschow, and F. Grandjean (unpublished).
[25] A. Ruderman and C. Kittel, Phys. Rev. **96**, 99 (1954).
[26] T. Kasuya, Prog. Theor. Phys. **16**, 45 (1956).
[27] K. Yosida, Phys. Rev. **106**, 893 (1957).
[28] M. B. Stearns, J. Appl. Phys. **35**, 1095 (1964).
[29] M. B. Stearns, Phys. Rev. **147**, 439 (1966).
[30] A. M. van der Kraan and K. H. J. Buschow, Physica B **138**, 55 (1986).
[31] J. W. C. de Vries, R. C. Thiel, and K. H. J. Buschow, J. Phys. F **14**, 2403 (1985).
[32] J. Pszczola, J. Zukrowki, J. Suwalski, Z. Kuchaarski, and M. Lukasiak, J. Magn. Magn. Mater. **40**, 197 (1983).
[33] R. H. Herber, in *Chemical Mössbauer Spectroscopy*, edited by R. H. Herber (Plenum, New York, 1984), p. 199.
[34] G. J. Long, G. K. Marasinghe, S. Mishra, O. A. Pringle, F. Grandjean, K. H. J. Buschow, D. P. Middleton, W. B. Yelon, F. Pourarian, and O. Isnard, Solid State Commun. **88**, 761 (1993).
[35] F. E. Wagner and G. Wortmann, in *Hydrogen in Metals I*, edited by G. Alefeld and J. Volkl (Springer, Berlin, 1977).
[36] F. S. Li, J. J. Sun, C. L. Yang, R. J. Zhou, B. G. Shen, H. Micklitz, and M. M. Abd-Elmeguid, Hyperfine Interactions **94**, 1959 (1994).
[37] H. Akai, S. Blügel, R. Zeller, and P. H. Dederiches, J. Magn. Magn. Mater. **54**, 1101 (1986).